Crystal Structures of [Fe]-Hydrogenase from Methanolacinia paynteri Suggest a Path of the FeGP-Cofactor Incorporation Process

Article *in* Inorganics · September 2020

CITATIONS
0

READS
20

4 authors, including:

Gang-Feng Huang
Max Planck Institute for Terrestrial Microbiology
13 PUBLICATIONS **81** CITATIONS

SEE PROFILE

inorganics

MDPI

Article

Crystal Structures of [Fe]-Hydrogenase from *Methanolacinia paynteri* Suggest a Path of the FeGP-Cofactor Incorporation Process

Gangfeng Huang [1], Francisco Javier Arriaza-Gallardo [1], Tristan Wagner [1,2] and Seigo Shima [1,*]

[1] Microbial Protein Structure Group, Max Planck Institute for Terrestrial Microbiology, Karl-von-Frisch-Straße 10, 35043 Marburg, Germany; gangfeng.huang@mpi-marburg.mpg.de (G.H.); francisco.arriaza@mpi-marburg.mpg.de (F.J.A.-G.); twagner@mpi-bremen.de (T.W.)

[2] Max Planck Research Group Microbial Metabolism, Max Planck Institute for Marine Microbiology, 28359 Bremen, Germany

* Correspondence: shima@mpi-marburg.mpg.de; Tel.: +49-6421-178100

Received: 18 August 2020; Accepted: 15 September 2020; Published: 17 September 2020

Abstract: [Fe]-hydrogenase (Hmd) catalyzes the reversible heterolytic cleavage of H_2, and hydride transfer to methenyl-tetrahydromethanopterin (methenyl-H_4MPT$^+$). The iron-guanylylpyridinol (FeGP) cofactor, the prosthetic group of Hmd, can be extracted from the holoenzyme and inserted back into the protein. Here, we report the crystal structure of an asymmetric homodimer of Hmd from *Methanolacinia paynteri* (pHmd), which was composed of one monomer in the open conformation with the FeGP cofactor (holo-form) and a second monomer in the closed conformation without the cofactor (apo-form). In addition, we report the symmetric pHmd-homodimer structure in complex with guanosine monophosphate (GMP) or guanylylpyridinol (GP), in which each ligand was bound to the protein, where the GMP moiety of the FeGP-cofactor is bound in the holo-form. Binding of GMP and GP modified the local protein structure but did not induce the open conformation. The amino-group of the Lys150 appears to interact with the 2-hydroxy group of pyridinol ring in the pHmd–GP complex, which is not the case in the structure of the pHmd–FeGP complex. Lys150Ala mutation decreased the reconstitution rate of the active enzyme with the FeGP cofactor at the physiological pH. These results suggest that Lys150 might be involved in the FeGP-cofactor incorporation into the Hmd protein in vivo.

Keywords: [Fe]-hydrogenase; FeGP cofactor; guanylylpyridinol; conformational changes; X-ray crystallography

1. Introduction

[Fe]-hydrogenase (Hmd) catalyzes the reversible hydride transfer to methenyl-tetrahydromethanopterin (methenyl-H_4MPT$^+$) from H_2 (Figure 1a) [1,2]. This reaction is involved in the hydrogenotrophic methanogenic pathway [2,3]. [Fe]-hydrogenase forms homodimer and contains an active site cleft at the two dimeric interfaces (Figure 1b) [4,5]. The active-site cleft binds the iron-guanylylpyridinol (FeGP) cofactor as the prosthetic group (Figure 1c) [6]. The FeGP cofactor contains a low spin Fe(II), which is ligated with two CO, one acyl-C and pyridinol nitrogen [5,7–12]. This cofactor is covalently bound to the protein via cysteine-S ligand at the iron site [5,10,13] (Figure 1c). The pyridinol ring is substituted with two methyl- and one guanosine monophosphate (GMP) groups [8]. The GMP part is bound to the mononucleotide-binding site of the Rossmann-fold-like structure of the Hmd protein [4].

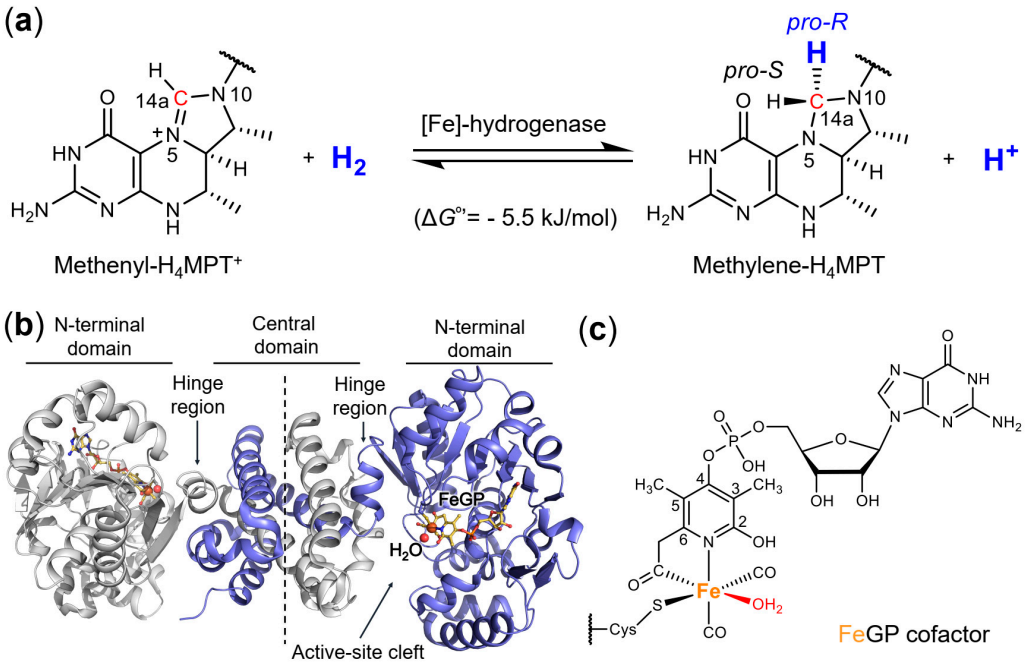

Figure 1. Structure and function of [Fe]-hydrogenase. (**a**) Reaction catalyzed by [Fe]-hydrogenase. The side chain of H_4MPT was omitted. (**b**) Crystal structure of [Fe]-hydrogenase (holoenzyme) from *Methanococcus aeolicus* (PDB: 6HAC). Two monomers are shown as a cartoon model (grey and blue). The FeGP cofactor is depicted as a ball and stick model. A water molecule is bound to the iron in the open resting state. (**c**) Chemical structure of the FeGP cofactor. Cys176 thiolate is covalently bound to the iron of the cofactor.

The FeGP cofactor is extractable from [Fe]-hydrogenase in the presence of 60% methanol, 1-mM 2-mercaptoethanol and 1% NH_3 [14]. The isolated cofactor is stabilized by 2-mercaptoethanol, which makes a complex at the iron site [10,12,15]. The FeGP cofactor can also be isolated in the presence of 50% acetic acid. An acetate ligand binds to the iron site to stabilize the iron complex of the cofactor [12]. The FeGP cofactor is decomposed by UV-A/blue light [16] and hydrogen peroxide [17,18]. A decomposition product of the organic part of the FeGP cofactor is guanylylpyridinol (GP), in which the acyl-methyl substituent was hydrolyzed to a carboxymethyl group [12].

Hmd proteins can be heterologously produced in *Escherichia coli* as an apo-form that does not contain the FeGP cofactor [19]. Crystal structure of the apo-Hmd from *Methanocaldococcus jannaschii* indicated that the active-site cleft of the apoenzyme is in a closed conformation [4]. When the extracted FeGP cofactor is mixed with the apoenzyme, the cofactor binds to the protein in the active-site cleft and generates the active holoenzyme [19]. Crystal structures of holoenzymes without substrate bound have always been observed in an open conformation, in which the active-site cleft is exposed to bulk solvent [5]. The structure of the Hmd from *Methanococcus aeolicus* holoenzyme in complex with methenyl-H_4MPT$^+$ showed that upon binding of methenyl-H_4MPT$^+$, the active-site cleft closes [20]. In the closed tertiary complex, the iron site of the FeGP cofactor is activated by expulsion of the water molecule bound on the iron site. The empty iron coordination site is proposed to be the H_2-binding site [20].

Many mimic complexes of the FeGP cofactor have been synthesized [2,21–26]. Some of the mimics are composed of similar complex structures to the FeGP cofactor containing Fe(II) [27] or Mn(I) [25] as the metal center with two CO and pyridinol but lack the GMP moiety. Several mimic complexes exhibit catalytic activities of H_2 activation and hydride transfer to chemical compounds [22–25]. Recently, reconstituted active semi-synthetic [Fe]-hydrogenases were produced by incorporation of the mimic complexes to the apoenzyme [25,28]. The reconstituted enzyme exhibited only a few percent of the activity of the native enzyme [28]. The reconstitution requires a longer period than that with the FeGP

cofactor to achieve full activity [28]. Addition of GMP during the reconstitution of the mimic-complexes increased the enzymatic activity to a certain extent [28].

In this work, we heterologously produced the Hmd apo-form from a mesophilic methanogenic archaeon, *Methanolacinia paynteri* (pHmd, National Center for Biotechnology Information Reference Sequence: WP_048153035.1), which belongs to the *Methanomicrobiales* order. The structures of Hmd from the *Methanomicrobiales* order have not been reported so far. We crystallized pHmd after in vitro reconstitution with the isolated FeGP cofactor from native Hmd purified from *Methanothermobacter marburgensis* [14]. These crystallization trials yielded two unexpected structures. The first one was an asymmetric pHmd homodimer containing one monomer bound with the FeGP cofactor and the other monomer in the apo-form. The second crystal structure was a symmetric homodimer in complex with the broken product of the FeGP cofactor (GP). In addition, co-crystallization experiments of pHmd with GMP and an iron mimic complex (see Section 3) yielded a symmetric homodimer in complex with only GMP. The crystal structures of asymmetric Hmd, and Hmd bound with GMP or GP have not been reported before. Based on the structures, we propose a possible trajectory of the binding process of the FeGP cofactor to the protein to produce the active holoenzyme.

2. Results and Discussion

2.1. Crystal Structure of the Asymmetric Homodimer of pHmd

Reconstitution of the pHmd holoenzyme was performed in the presence of a slight excess of FeGP cofactor (0.18 mM) relative to the pHmd protein (0.13 mM). The specific activity of the reconstituted enzyme was variable in the holo-form obtained in each reconstitution experiment (60–250 U/mg at 40 °C) under standard assay conditions (oxidation of methylene-H_4MPT), which was substantially lower than that of the native Hmd from *M. marburgensis* (~400 U/mg at 40 °C) [14], the reconstituted Hmd from *Methanocaldococcus jannaschii* (jHmd) (~400 U/mg at 40 °C) [14], and the reconstituted Hmd from *Methanococcus aeolicus* (3000 U/mg at 40 °C) [20]. The 2.1 Å crystal structure obtained from this reconstituted preparation contained one homodimer in the asymmetric unit, in which one monomer is bound to the FeGP cofactor and the other is in an apo-form (Figure 2, Table 1). The active-site cleft bound with the FeGP cofactor was in the open conformation and the second monomer without the cofactor was in the closed conformation. The formation of the asymmetric structure indicated that the open/closed conformational change of a monomer of the Hmd homodimer occurs independently from another monomer.

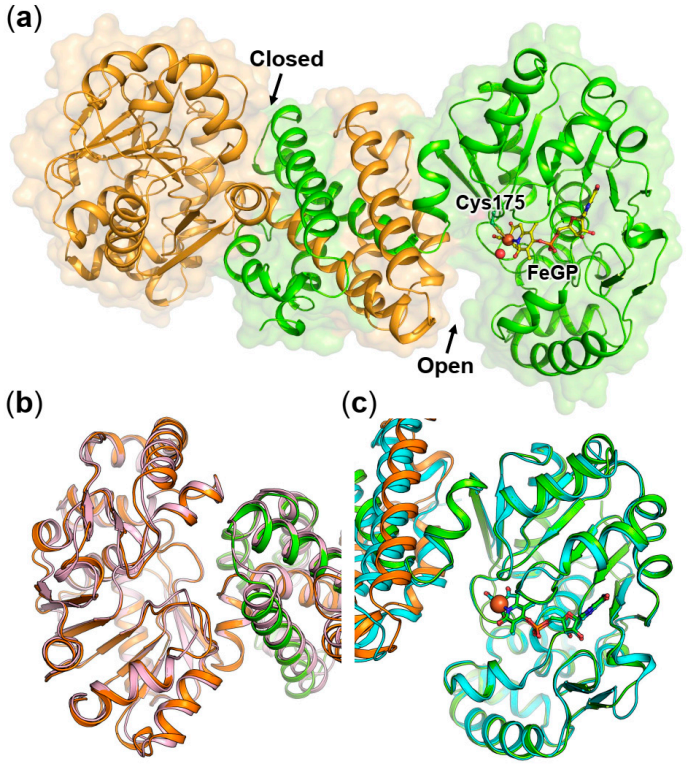

Figure 2. Crystal structure of the asymmetric homodimer of pHmd. (**a**) Overview of the asymmetric homodimer of pHmd. One monomer (left) is the apo-form and the second monomer (right) is bound to the FeGP cofactor. (**b**) Comparisons between the apo-form of the asymmetric pHmd homodimer (orange) and apo-form of jHmd (pink, PDB: 2B0J). The chain from the next monomer of pHmd in the central domain is distinguished by the green color. (**c**) Comparison between the holo-form of the asymmetric pHmd homodimer (green) and holo-form of jHmd (blue, PDB: 3F47). The chain from the next monomer of pHmd in the central domain is distinguished by the orange color. The FeGP cofactor is shown by ball and stick models. For both pictures in (**b**,**c**), the N-terminal domain is superposed.

Table 1. X-ray analysis statistics.

	Asymmetric Homodimer-pHmd	GMP Bound	GP Bound
Data collection			
Wavelength (Å)	0.97980	0.97972	0.97970
Space group	$P3_121$	$P2_1$	$C2$
Resolution (Å)	45.13–2.10 (2.21–2.10)	43.65–1.55 (1.63–1.55)	46.63–1.70 (1.79–1.70)
Cell dimensions			
a, b, c (Å)	79.48, 79.48, 179.34	67.81, 57.06, 95.13	160.83, 93.27, 83.64
α, β, γ (°)	90, 90, 120	90, 91.43, 90	90, 97.53, 90
Nr. Monomers/asym. Unit	2	2	4
open/closed conformation	1 + 1	0/2	0/4
R_{merge} (%) [a]	5.9 (71.1)	6.8 (35.3)	10.7 (51.7)
R_{pim} (%) [a]	1.9 (22.2)	4.1 (21.3)	6.5 (30.8)
$CC_{1/2}$ [a]	1.000 (0.755)	0.997 (0.653)	0.993 (0.605)
I/σ_I [a]	28.8 (3.6)	12.6 (3.7)	8.0 (2.5)
Completeness (%) [a]	100.0 (100.0)	99.3 (99.7)	99.1 (99.1)
Redundancy [a]	10.8 (11.1)	3.7 (3.7)	3.7 (3.8)
Nr. unique reflections [a]	39,181 (5643)	104,812 (15285)	133,035 (19398)
Refinement			

Table 1. *Cont.*

	Asymmetric Homodimer-pHmd	GMP Bound	GP Bound
Resolution (Å)	39.74–2.10	22.69–1.55	24.89–1.70
Number of reflections	39,126	104,777	132,993
R_{work}/R_{free} [b] (%)	19.5/23.5	18.4/20.9	18.9/21.6
Number of atoms			
Protein	5215	5256	10,490
Ligands/ions	103	78	114
Solvent	224	640	1068
Mean B-value ($Å^2$)	61.9	22.2	23.1
Molprobity clash score, all atoms	1.49	1.39	0.79
Ramachandran plot			
Favored regions (%)	97.05	96.31	96.31
Outlier regions (%)	0.15	0	0
Rmsd [c] bond lengths (Å)	0.008	0.010	0.010
Rmsd [c] bond angles (°)	1.01	1.10	1.08
PDB code	6YKA	6YKB	6YK9

[a] Values relative to the highest resolution shell are within parentheses. [b] R_{free} was calculated as the R_{work} for 5% of the reflections that were not included in the refinement. [c] rmsd, root mean square deviation.

The N- (residues 1–241) and C- (residues 253–342) terminal domains of the two monomers of the asymmetric homodimer are very similar to each other: 217 Cα superposed with a root mean square deviation (rmsd) of 0.192 Å for the N-terminal domain and 74 Cα superposed with a rmsd of 0.131 Å for the C-terminal domain. The N-terminal domains of the apo- and holo-form monomers of the asymmetric pHmd overlapped with those of apo- and holo-forms of Hmd from *M. jannaschii* (jHmd), respectively (Figure 2b,c). However, when the central domain composed of the dimeric C-terminal domains are superposed, a deviation of the N-terminal domain is observed between pHmd apo- and holo-forms compared to those of apo- and holo-forms of jHmd, respectively (Figure S1). Such variation is caused by the asymmetric structure; the holo conformation impacts the apo conformation at the central domain and vice versa.

According to the similar N-terminal domain structures, the holo-form of pHmd shows an identical binding mode of the FeGP cofactor as observed in the jHmd holoenzyme (Figure S2). In contrast, the apo-forms of pHmd and jHmd showed a slight difference at the loop involved in the FeGP cofactor coordination. One of the differences between the pHmd and jHmd apo-forms is the location of Lys150, which moved outside from the active site in jHmd (Figure S3). This movement might also be attributed to the crystal packing. Lys150 is conserved in the Hmd-encoding genes in the genomes reported with exceptions found in fifteen genomes of *Methanobrevibacter* species (e.g., *M. smithii*), where the lysine position varies to glutamate (Figure S4). Notably, the Hmd activity of the cell extract from the *Methanobrevibacter* species was very low [29,30].

2.2. Crystal Structure of pHmd in Complex with GMP

We obtained crystals from the solutions containing the reconstituted pHmd with an iron complex in the presence of GMP. This mimic complex has been used for reconstitution of semisynthetic jHmd (see Section 3) [28]. The 1.55 Å crystal structure revealed a symmetric pHmd homodimer in the closed conformation, which was fully occupied with GMP but without mimic complex (Figure 3, Table 1). The N-terminal domain of the GMP-binding structure and the apo-form monomer of pHmd in the asymmetric homodimer superposed well (295 Cα superposed with rmsd of 0.416 Å, Figure 3a). The GMP binding site is identical to that of the FeGP cofactor observed in the pHmd–FeGP complex of the asymmetric pHmd. The residues in direct contact with GMP and the GMP moiety of the FeGP cofactor have the same orientations (Figure 3b). The Lys150 side chain adopts the same orientation as in the apo form; however, binding of the GMP slightly rearranged the loop 110–116 and rigidified its surroundings as observed by a lower B-factor profile.

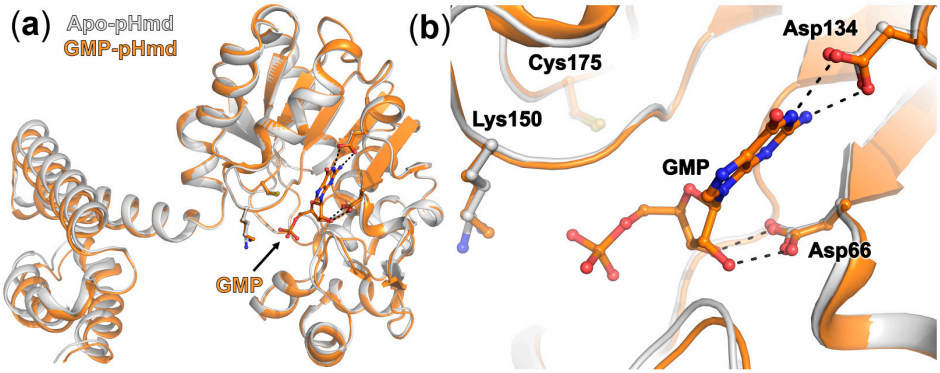

Figure 3. Structural comparison of the apo-form of the pHmd asymmetric-homodimer (grey) and the GMP-bound form (orange) of pHmd. (**a**) Monomers of each structure is shown by cartoon model. The N-terminal domains were superposed. (**b**) Zoom-up view of the GMP binding site. GMP is shown as ball and stick model. Hydrogen bonds are indicated by dashed lines.

2.3. Crystal Structure of pHmd in Complex with GP

From the reconstituted pHmd holoenzyme with the FeGP cofactor, in addition to the asymmetric homodimer crystal, another crystalline form was obtained. This form diffracted to 1.7 Å resolution (Table 1). The asymmetric unit of the crystal contained two homodimers in the closed conformation. Contrary to the other reconstituted holo-Hmd structures, the pyridinol part was only partially visible in the electron density and could be modelled for only one monomer in the four monomers in the asymmetric unit. The FeGP cofactor appeared to be decomposed to GP during crystallization process. The structures of the N-terminal domain and the residues binding GMP and GP superposed well (Figure 4a). Binding of GP induces the local conformational rearrangement of the two loops containing Lys150 and Cys175, respectively, compared to the apo form. In the pHmd–GP structure, the van der Waals interaction between the hydroxyl group of the pyridinol ring and amino group of Lys150 (2.7 Å) stabilizes the pyridinol ring of GP in this structure (Figure 4). The Cys175 side chain was modelled in two conformations of 80% and 20% occupancy in the broad electron density. The interaction between the amino group of Lys150 and the pyridinol does not appear to be optimal for hydrogen-bonding. However, in the incorporation process of the FeGP cofactor, a slight tilt of the pyridinol ring would improve the interaction.

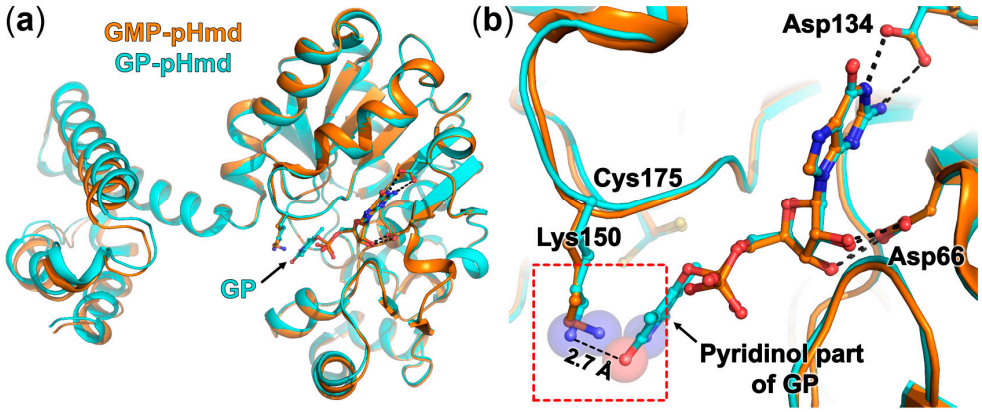

Figure 4. Structural comparison of the GMP-bound form (orange) and the GP-bound form (cyan) of pHmd. (**a**) Monomers of each structure are shown by a cartoon model. The N-terminal domains are superposed. (**b**) Zoomed-in view of the active site. GMP and GP are shown by ball and stick models. Hydrogen bonds are indicated by dashed lines.

The carboxymethyl part of the pyridinol group was not visible, which indicates that the elongated carboxymethyl substituent of the GP does not interact with the protein. This observation contrasts with the structure of hexameric Hmd from *M. marburgensis* in the open conformation obtained in an oxidized broken state. The carboxymethyl group was visible and bound with an Fe atom coordinated by His203 and Cys172, and Asp189 from loop of another dimer (Figure S5a) [18]. The loop containing Asp189 is not conserved in the pHmd sequence. The absence of the loop structure explains why the GP binding mode is different and the iron was removed from the cleft after decomposition (Figure S5b).

The closed conformation of the active-site cleft of the pHmd in complex with GP and also GMP indicated that binding of the GMP and pyridinol parts of the FeGP cofactor does not induce the opening of the active-site cleft. The formation of the Cys175-S–Fe bonding and the resulting conformational change of the loop at Cys175 might trigger the open state. The crystal structure of the reconstituted Cys176Ala-mutated jHmd holoenzyme (Cys176 of jHmd is equivalent to Cys 175 of pHmd) has been reported [10]. This enzymatically inactive jHmd holoenzyme, lacking the Cys176-S–Fe bonding, was crystallized in the open conformation even in the presence of methylene–H_4MPT bound, which indicated that the Cys176Ala mutation hindered the open/closed conformational change essential for the catalytic activity.

In the pHmd holo-form in the asymmetric homodimer, Lys150 is dissociated from the pyridinol ring and the loop containing Lys150 moved slightly away (Figure 5). Lys150 should move further away from the active site in the closed conformation induced by methenyl-H_4MPT$^+$ binding, because the Lys150 side chain clashes with the phenyl ring part of methenyl-H_4MPT$^+$ observed in the holoenzyme structure Hmd from *Methanococcus aeolicus* in complex with methenyl-H_4MPT$^+$ (Figure S6) [20]. In the ternary complex, the Lys150 comes into contact with the side chain of methenyl-H_4MPT$^+$, mainly via a water network, which might therefore have an additional role in the substrate binding.

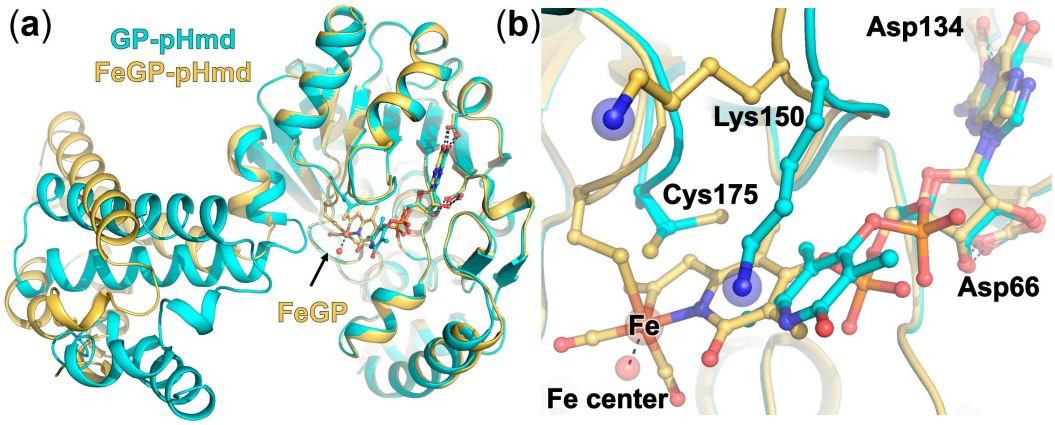

Figure 5. Structural comparison of the GP-bound form (cyan) of pHmd and the FeGP-bound form (yellow) of the pHmd asymmetric homodimer. (**a**) Monomers of each structure are shown by a cartoon model. The N-terminal domains were superposed. (**b**) Zoomed-in view of the active site. GP and FeGP are shown by ball and stick models. In the GP-bound form, the carboxymethyl group of GP is not visible. Hydrogen bonds are indicated by dashed lines.

2.4. Effect of Lys150Ala Substitution on the Reconstitution Rate of pHmd

The structural analysis of pHmd in complex with GP indicated that Lys150 could interact with the FeGP cofactor in the incorporation process. This hypothesis was tested using the pHmd Lys150Ala variant. Prior to the reconstitution assay, we measured the kinetic parameters of the wild-type enzyme and Lys150Ala variant reconstituted under the standard reconstitution condition. Unexpectedly, the Lys150Ala variant exhibited much higher V_{max} and K_m values (640 U/mg and 160 μM) than those of the wild-type enzyme (66 U/mg and 6 μM) in the oxidation reaction of methylene-H_4MPT at pH 6.0 (Figures S7 and S8). The V_{max} and K_m of the reduction reaction of methenyl-H_4MPT$^+$ with H_2 at pH 7.5 are 1300 U/mg and 62 μM for the wild-type enzyme and 820 U/mg and 110 μM for the K150A variant, respectively. Increase of the K_m values of the Lys150Ala variant is consistent with the observation of the contact of Lys150 with the side chain of methenyl-H_4MPT described in the last section.

The formation of the holoenzyme by binding of the FeGP cofactor was followed by monitoring the increase of enzymatic activity after addition of the FeGP cofactor (4–700 nM) to the assay solution, which contained the 4-nM apoenzyme, and 20-μM methenyl-H_4MPT$^+$ under H_2 at pH 7.5 or 20-μM methylene–H_4MPT under N_2 at pH 6.0. The time course of the change of the absorbance at 336 nm was recorded (Figure 6a,b,e,f). We calculated the specific activity (U/mg) at each time point (per 2 s) from the slope of the absorbance change (Figure 6c,d,g,h). In these experiments, we assume that the increase of the Hmd activity indicates the increase of the active holoenzyme in the assay by incorporation of the FeGP cofactor into the apoenzymes. Hence, the specific activity is a function of the concentration of the reconstituted enzyme and the residual substrate concentration in the assay. In the assay condition at pH 7.5, which is the physiological pH [31], the wild-type enzyme was quickly reconstituted and reached the maximum activity within 25 s in the presence of 700-nM FeGP cofactor (Figure 6c). The Lys150Ala variant also exhibits activity, but the increase of the specific activity at the same condition was much slower than the case of the wild-type enzyme; to reach the maximal activity, 130 s was required (Figure 6d). These results support the hypothesis that Lys150 contributes to the binding kinetics of the FeGP cofactor to the protein. In the case of the reverse reaction, oxidation of methylene–H_4MPT at pH 6.0, the Lys150Ala mutation did not affect the reconstitution of the holoenzyme (Figure 6e–h). To obtain the reconstitution rate from the data, we simulated the reconstitution curves (Figures S9 and S10). The simulated curves of reconstitution fitted to the observed curve when the reconstitution rate (k_2 in Figure S9) of the FeGP cofactor to the wild and Lys150Ala apoenzymes are assumed as 0.01 ± 0.005 $\mu M^{-1} \cdot s^{-1}$ and 0.0024 ± 0.0003 $\mu M^{-1} \cdot s^{-1}$ at pH 7.5 and 0.10 ± 0.01 $\mu M^{-1} \cdot s^{-1}$ and 0.14 ± 0.03 $\mu M^{-1} \cdot s^{-1}$ at pH 6.0, respectively. These data support the function of Lys150 in the binding kinetics of incorporation of the FeGP cofactor in the physiological pH. Protonation of the 2-hydroxy group of the FeGP cofactor might affect the incorporation rate of the FeGP cofactor into the protein.

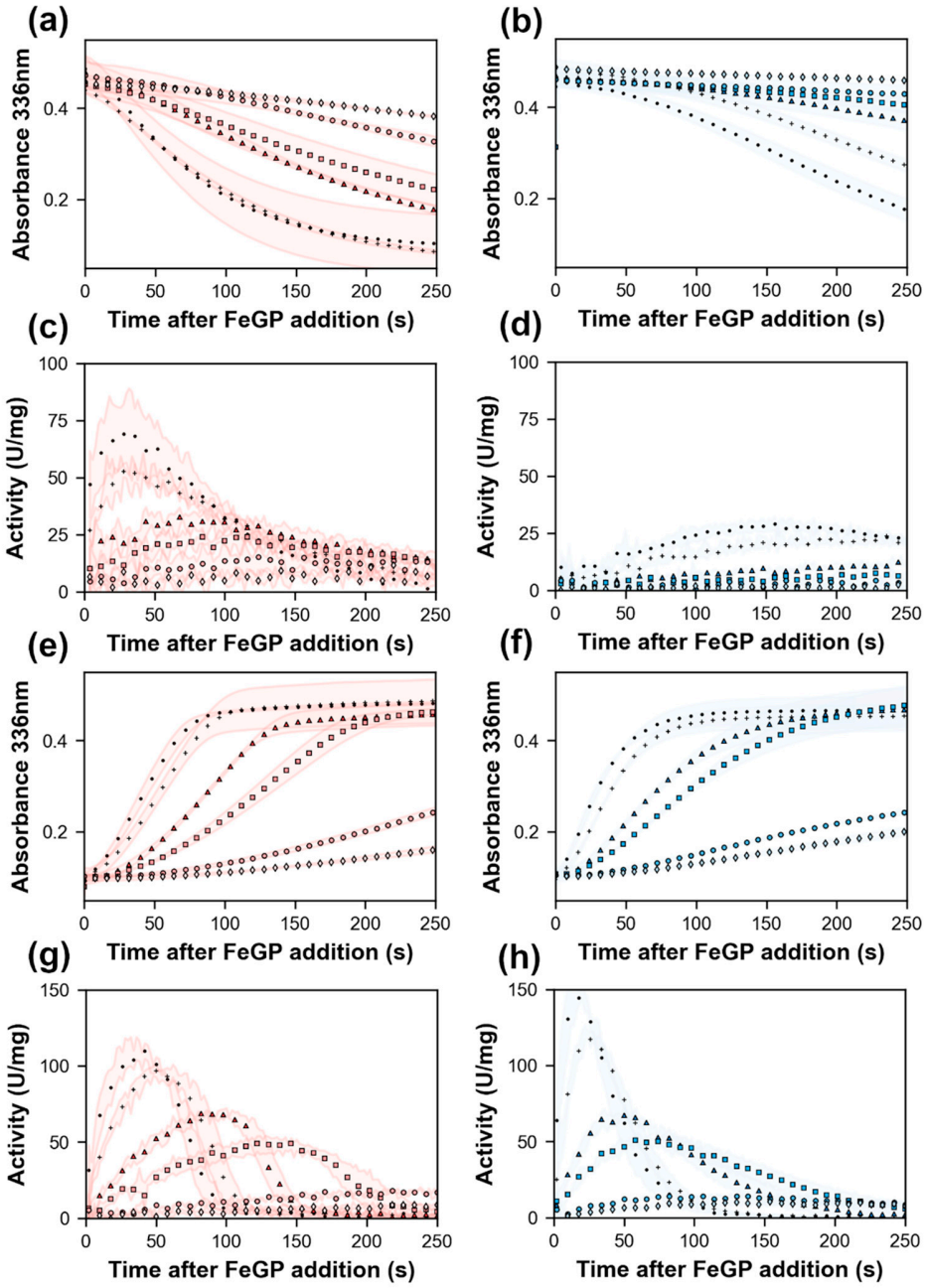

Figure 6. Reconstitution of the [Fe]-hydrogenase holoenzyme from the apoenzyme of the wild-type (**a**,**c**,**e**,**g**) and Lys150Ala variant (**b**,**d**,**f**,**h**) with the FeGP cofactor. Changes of the absorbance at 336 nm according to the reduction of methenyl-H_4MPT^+ (**a**,**b**) and oxidation of methylene-H_4MPT (**e**,**f**) were recorded. The color area indicates the standard deviation of three tests. The enzymatic activity (U/mg) (**c**,**d**,**g**,**h**) of each 2 s was calculated from the data of (**a**,**b**,**e**,**f**), respectively. Concentrations of the FeGP cofactor were 700 (•), 350 (+), 100 (Δ), 50 (□), 10 (○) and 4 nM (◊). The plots of the data of the wild type and the Lys150Ala variant are shown in red and blue, respectively.

3. Materials and Methods

3.1. Chemicals and Reagents

Tetrahydromethanopterin (H_4MPT) and methenyl-H_4MPT^+ were isolated from *M. marburgensis* cells [32]. Methylene-H_4MPT was produced by the reaction of H_4MPT with formaldehyde [14]. The FeGP

cofactor was isolated from [Fe]-hydrogenase from *M. marburgensis* as described previously [14]. All other chemical compounds used in this work were purchased from Sigma-Aldrich (Darmstadt, Germany).

3.2. Gene Synthesis of [Fe]-Hydrogenase from Methanolacinia Paynteri

The [Fe]-hydrogenase gene from *M. paynteri* (NCBI Reference Sequence: WP_048153035.1) was modified for the codon usage optimization as shown below and synthesized by GenScript. The DNA synthesized was inserted into the expression vector pET-24b(+) at the *Nde*I and *Sal*I restriction-enzyme digestion sites. Genes of the Lys150Ala variant were synthesized using the template of the wild-type gene.

5′-CATATGACAATAAAGAAGGTAGCTATACTAGGAGCAGGGTGTTATAGGACTCACTCA
GCGACCGGCATTACCAACTTTGCGCGTGCGTGCGAGGTGGCGGAAATGGTTGGTAAACCGG
AGATCGCGATGACCCACAGCACCATTGCGATGGCGGCGGAACTGAAGTACCTGGCGGGCAT
CGACAACATCGTGATTAGCGATCCGAGCTTCGCGGGCGAGTTTACCGTGGTTAAGGACTTCG
ATTACAACGAAGTTATCAAGGCGCACAAAGAGAACCCGGAAACCATCATGCCGAAGATTCGT
GAGAAAGTGAACGAACTGGCGAAAACCGTTCCGAAGCCGCCGAAAGGCGCGATCCACTTTG
TGCACCCGGAGGACCTGGGTCTGAAGGTGACCACCGACGATCGTGAAGCGGTTCGTGACG
CGGATCTGATCATTACCTGGCTGCCGAAGGGTGACATGCAGAAAGGCATCATTGAGAAGTTC
GCGGGTGATATCAAGCAAGGCGCGATCATTACCCACGCGTGCACCATTCCGACCACCCTGTT
CTACAAAATCTTTGAGGAACTGGGCATTGCGGATAAGGTGGAAGTTACCAGCTATCACCCGG
GTGCGGTGCCGGAGATGAAAGGCCAGGTTTACATCGCGGAAGGTTATGCGAGCGAGGAAGC
GATCAACACCATTTACGAGCTGGGTAAGAAAGCGCGTGGTCATGCGTTTAAGCTGCCGGCGG
AACTGATTGGTCCGGTTTGCGACATGTGCGCGGCGCTGACCGCGATTACCTACGCGGGTCTG
CTGGTGTATCGTGATGCGGTTATGAACATTCTGGGTGCGCCGGCGGGTTTCAGCCAGATGAT
GGCGACCGAGAGCCTGGAACAAATCACCGCGTATATGAAGAAAGTGGGTATTAAAAACCTGG
AGGAAAACCTGGACCCGGGTGTTTTCCTGGGCACCGCGGATAGCATGAACTTTGGCCCGATT
GCGGAGATTCTGCCGACCGTTCTGAAGAGCCTGGAAAAGCGTGCGAAATAAGTCGAC-3′.

3.3. Enzyme Production, Purification and Reconstitution

The apoenzymes of [Fe]-hydrogenase from *M. paynteri* were heterologously overproduced in *E. coli* BL21(DE3). The recombinant *E. coli* was cultivated in the tryptone–phosphate (TP) medium containing 50 µg/mL kanamycin at 37 °C [33]. When the optical density of *E. coli* at 600 nm became 0.6–0.8, 1-mM isopropyl β-D-thiogalactopyranoside (IPTG) was added to induce expression of the targeted gene. Cells were harvested by centrifugation using Avanti JXN-26 centrifuge with JLA-10.500 rotor (Beckman-Coulter, Krefeld, Germany) at 8000 rpm for 30 min at 4 °C. The wet cells (5–10 g) were suspended in 50-mM 3-(*N*-morpholino)propanesulfonic acid (MOPS)/KOH pH 7.0 containing 1-mM dithiothreitol (DTT). Cells were disrupted on ice by sonication for 10 min using SONOPULS GM200 (Bandelin, Berlin, Germany) with KE76 tip with 50 cycles. The cell debris and the unbroken cells were removed by centrifugation using an Avanti JXN-26 centrifuge with a JA-25.50 rotor (Beckman-Coulter) at 15,000 rpm for 30 min at 4 °C. Ammonium sulfate (2-M final concentration) was added to the supernatant. Precipitates were removed by centrifugation using an Avanti JXN-26 centrifuge with JA-25.50 rotor at 15,000 rpm for 30 min at 4 °C. The supernatant was loaded on a Phenyl Sepharose High Performance column (75 mL, GE Healthcare Life Sciences, Solingen, Germany) and eluted with a linear gradient of ammonium sulfate from 2 M to 0 M in 50-mM MOPS/KOH buffer pH 7.0 containing 1-mM DTT. Fractions containing the apoenzyme of pHmd were collected and concentrated by using Amicon Ultra-4 Centrifugation filters (30-kDa cut-off). To further purify the apoenzyme of pHmd, the concentrated apoenzyme sample was loaded to a HiPrep 16/60 Sephacryl S-200 HR gel filtration column (120 mL, GE Healthcare Life Sciences) using 25-mM Tris(hydroxymethyl)aminomethane (Tris)/HCl buffer pH 7.5 containing 150-mM NaCl, 5% glycerol and 2-mM DTT. To increase the purity of protein, the gel filtration repeated two times using the same conditions [20]. Finally, the purified apoenzyme was concentrated to 50–100 mg/mL.

Protein concentration was measured by Bradford method using bovine serum albumin as the standard. Reconstitution was performed under dark conditions in an anoxic tent (Coy) with a gas phase of 95%N_2/5%H_2 at 8 °C by mixing the 0.13-mM apoenzyme and the 0.18-mM FeGP cofactor (at a molecular ratio of 0.75:1), respectively, as previously described [14].

3.4. Enzyme Activity Assay

The enzyme activity was anaerobically measured as previously described using a 1-mL quartz cuvette containing 0.7 mL assay mixture [14]. For the reduction of methenyl-H_4MPT^+ with H_2, 120-mM potassium phosphate pH 7.5 containing 1-mM ethylenediaminetetraacetic acid (EDTA) was used as the assay buffer under 100% H_2. For the oxidation of methylene-H_4MPT under N_2, 120-mM potassium phosphate pH 6.0 containing 1-mM EDTA was used as assay buffer under 100% N_2. The assay was started by adding 10 µL of 0.01 mg/mL enzyme solution (final concentration in the assay was 0.14 µg/mL), and the decrease (reduction)/increase (oxidation) of absorbance at 336 nm was recorded. Its specific activity was calculated using the extinction coefficient of methenyl-H_4MPT^+ (ε_{336nm} = 21.6 $mM^{-1}{\cdot}cm^{-1}$) [14]. One unit (U) activity is the amount of the enzyme catalyzing the formation or consumption/formation of 1 µmol methenyl-H_4MPT per min.

The reconstitution rate of the holoenzyme was kinetically analyzed in a quartz cuvette. The assay solution for the reduction reaction contained 120-mM potassium phosphate buffer pH 7.5, 1-mM EDTA, 4-nM (0.15 µg/mL) pHmd apoenzyme and 20-µM methenyl-H_4MPT^+ under 100% H_2. In the oxidation reaction, the assay solution contained 120-mM potassium phosphate buffer pH 6.0, 1-mM EDTA, 4-nM (0.15 µg/mL) pHmd apoenzyme and 20-µM methylene-H_4MPT under 100% N_2 The reaction was started by the addition of 4–700-nM cofactor (final concentration). A change of the absorbance at 336 nm was recorded at 40 °C.

3.5. Simulation of the Enzyme Kinetics Data

Michalis–Menten kinetics-parameters were obtained by simulation of the substrate consumption and product formation by numerical integration of the equations derived from mass action kinetics (Figure S7). The reconstitution rate with the FeGP cofactor and simulated enzymatic activities were calculated by numerical integration using the equations shown in Figure S9. All simulations were coded in Python 3.7 using Spyder 4.1 development environment and the following libraries: SciPy [34], NumPy [35], Matplotlib [36] and pandas [37].

3.6. Crystallization

[Fe]-hydrogenase holoenzyme from *M. paynteri* (pHmd) was crystallized under 95%N_2/5%H_2 at 8 °C using 96-well two-drop MRC crystallization plates (sitting drop vapor diffusion method). For the crystallization of pHmd–GP and pHmd–FeGP complexes, 0.7 µL of 25 mg/mL reconstituted holoenzyme was mixed with 0.7 µL reservoir solution (from crystallization kits) under yellow light and incubated under dark conditions. The best diffracting crystal of pHmd–GP came out within two weeks in 25% *w/v* polyethylene glycol 1500 and 100-mM succinic acid/sodium dihydrogen phosphate/Glycine (SPG) buffer pH 8.5 (JBScreen Wizard 3&4 HTS, Jena Bioscience, Jena, Germany). For pHmd asymmetric dimer form, the crystals grew within two weeks in 30% *w/v* polyethylene glycol 4000, 200-mM lithium sulfate and 100-mM Tris pH 8.5 (JBScreen Wizard 3&4 HTS, Jena Bioscience).

The reconstituted holoenzyme with the Fe complex was prepared as previously described [28]. An Fe(II) complex [(2-CH_2CO-6-HOC_5H_3N)$Fe(CO)_3I$] (complex 5 in [26]) was dissolved in methanol containing 1% acetic acid [28]. For reconstitution, 0.4 mL of 10-mM Fe complex solution was mixed anaerobically with a 7.6 mL solution of 100-mM sodium acetate pH 5.6, 0.02 mM apoenzyme and 2-mM GMP (final concentrations) and incubated on ice for one hour. The buffer of the reconstituted enzyme was exchanged by three-time concentration/dilution cycles using a 30 kDa ultrafilter with 10 mM MOPS/KOH pH 7.0 and finally concentrated to 25 mg/mL. For crystallization, 0.7 µL of the reconstituted pHmd solution was mixed with 0.7 µL reservoir solution (from crystallization kits) under

yellow light and incubated under dark conditions at 10 °C. The best crystal appeared within one month in 20% *w/v* polyethylene glycol 3350 and 200-mM magnesium formate reservoir solution (JBScreen Wizard 3&4 HTS, Jena Bioscience).

3.7. Data Collection and Refinement

The crystals of the asymmetric homodimer and the one containing GP were flash-frozen (3–5 s) in their crystallization reservoir solution supplemented with 10% *v/v* glycerol under 95%N_2/5%H_2. The crystal of pHmd bound with GMP was flash-frozen (3–5 s) in its crystallization reservoir solution containing 30% *v/v* glycerol under 95%N_2/5%H_2. All diffraction experiments were performed at 100 K on beamline BM30A (French Beamline for Investigation of Proteins) at the European Synchrotron Radiation Facility (ESRF) equipped with an ADSC Q315r charge-coupled device detector. The data were processed with XDS [38] and scaled with SCALA from the CCP4 suite [39]. The structure of pHmd–FeGP was determined by molecular replacement with PHASER [40] by decoupling the N- and C-terminal domain of the native Hmd from *M. marburgensis* in complex with 2-naphthylisocyanide (PDB: 4JJF) as templates. The structures of pHmd–GP and pHmd–GMP were solved with PHASER by using the monomer in the closed conformation of the asymmetric homodimer. The models were manually built with COOT [41] and refined with Phenix [42] and BUSTER (Bricogne G., Blanc E., Brandl M., Flensburg C., Keller P., Paciorek W., Roversi P, Sharff A., Smart O.S., Vonrhein C., Womack T.O. (2017). BUSTER version 2.10.3. Cambridge, United Kingdom: Global Phasing Ltd.). The final models were validated using the MolProbity server (http://molprobity.biochem.duke.edu) [40]. Data collection, refinement statistics and PDB code for the deposited model are listed in Table 1. The hydrogens were omitted in the final deposited model. The figures were generated and rendered with PyMOL (version 1.7, Schrödinger, Cambridge, UK). Alignments were performed by Clustal Omega [43]. The figures were made using ESPript 3.0 [44].

4. Conclusions

Based on the crystal structures of the pHmd apo- and holo-form—the latter bound with GMP, GP or the FeGP cofactor—we propose a trajectory of the isolated FeGP cofactor incorporation into the apoenzyme. First, binding of the GMP part guides correct positioning of the FeGP cofactor, which slightly opens the active-site cleft to engage the binding of the pyridinol part at the flexible Cys175 loop and induces small local conformational change at the loop containing Lys150. The iron site of the FeGP cofactor forms a covalent Cys175-S–Fe bonding upon exchange with the acetate/2-mercaptoethanol ligand bound in the free cofactor. Sequential binding of the GMP and pyridinol moieties might allow a correct covalent bonding between Cys175-thiolate and the Fe site. Lys150 might guide the binding of the pyridinol part to the specific position. The Lys150Ala mutation analysis supported this hypothesis. These results are of general interest for studying how nucleotide-containing cofactors and coenzymes are incorporated into the protein, and for developing semi-synthetic [Fe]-hydrogenase using mimic complexes. A plausible strategy of incorporation of the mimic complexes into the Hmd protein is to synthesize mimic compounds, which contains the GMP moiety at the position 4 of the pyridinol ring. Another strategy might be modifying the Hmd apoenzyme to enhance a smooth Fe–S bond formation of the mimic cofactor in the absence of the GMP moiety, in which the loop containing Lys150 might be the target of modification.

Supplementary Materials: The following are available online at http://www.mdpi.com/2304-6740/8/9/50/s1, Figure S1. Observation of subtle rearrangements of the asymmetric pHmd when the C-terminal domain of holo-jHmd and apo-jHmd are superposed, Figure S2. Superposition of the FeGP cofactor binding sites in pHmd (PDB: 6YKA), Hmd from *Methanococcus aeolicus* (aHmd) (PDB: 6HAC) and jHmd (PDB: 3F47), Figure S3. Comparison of the loop involved in the FeGP cofactor coordination in the jHmd and pHmd apo-forms. Figure S4. Alignments of Hmd amino acid sequences from different organisms, Figure S5. Comparison of the GP-binding states in the structure of Hmd from *M. marburgensis* obtained in an oxidized broken state with that in the structure of GP bound form of pHmd, Figure S6. Superposition of the active sites of apo- and holo-forms of Hmd. Figure S7. Equations used for the simulation of the modelled reaction and calculation of the kinetic parameters. Figure S8. Simulation of the progressive curves of the reactions. Figure S9. Equations used for the simulation of the binding

constant of the FeGP cofactor to the pHmd apoenzyme, Figure S10. Simulation of the change of the activity in the reconstitution assay of pHmd.

Author Contributions: Conceptualization, S.S.; methodology, S.S.; software, T.W.; validation, T.W.; formal analysis, G.H., T.W., F.J.A.-G. and S.S.; investigation, G.H., T.W. and F.J.A.-G.; resources, S.S..; data curation, G.H., F.J.A.-G., T.W. and S.S.; writing—original draft preparation, S.S.; writing—review and editing, G.H., F.J.A.-G., T.W. and S.S.; visualization, G.H and T.W.; supervision, S.S.; project administration, S.S.; funding acquisition, S.S. and T.W. All authors have read and agreed to the published version of the manuscript.

Funding: This work was funded by the Max Planck Society (to T.W. and S.S.) and the Deutsche Forschungsgemeinschaft priority program (SPP 1927) (SH 87/1-1, to S.S.).

Acknowledgments: We thank Xile Hu (École polytechnique fédérale de Lausanne), who provided us the iron complex. The authors thank the staff from the BM30A (FIP) beamline at the European Synchrotron Radiation Facility (ESRF) for their availability and advice during data collection.

Conflicts of Interest: The authors declare no conflict of interest.

References

1. Zirngibl, C.; van Dongen, W.; Schwörer, B.; von Bünau, R.; Richter, M.; Klein, A.; Thauer, R.K. H_2-forming methylenetetrahydromethanopterin dehydrogenase, a novel type of hydrogenase without iron-sulfur clusters in methanogenic archaea. *Eur. J. Biochem.* **1992**, *208*, 511–520.
2. Huang, G.F.; Wagner, T.; Ermler, U.; Shima, S. Methanogenesis involves direct hydride transfer from H_2 to an organic substrate. *Nat. Rev. Chem.* **2020**, *4*, 213–221.
3. Shima, S.; Huang, G.; Wagner, T.; Ermler, U. Structural basis of hydrogenotrophic methanogenesis. *Annu. Rev. Microbiol.* **2020**, *74*, 713–733.
4. Pilak, O.; Mamat, B.; Vogt, S.; Hagemeier, C.H.; Thauer, R.K.; Shima, S.; Vonrhein, C.; Warkentin, E.; Ermler, U. The crystal structure of the apoenzyme of the iron-sulphur cluster-free hydrogenase. *J. Mol. Biol.* **2006**, *358*, 798–809.
5. Shima, S.; Pilak, O.; Vogt, S.; Schick, M.; Stagni, M.S.; Meyer-Klaucke, W.; Warkentin, E.; Thauer, R.K.; Ermler, U. The crystal structure of [Fe]-hydrogenase reveals the geometry of the active site. *Science* **2008**, *321*, 572–575.
6. Shima, S.; Ermler, U. Structure and function of [Fe]-hydrogenase and its iron-guanylylpyridinol (FeGP) cofactor. *Eur. J. Inorg. Chem.* **2011**, *2011*, 963–972.
7. Lyon, E.J.; Shima, S.; Boecher, R.; Thauer, R.K.; Grevels, F.W.; Bill, E.; Roseboom, W.; Albracht, S.P.J. Carbon monoxide as an intrinsic ligand to iron in the active site of the iron-sulfur-cluster-free hydrogenase H_2-forming methylenetetrahydromethanopterin dehydrogenase as revealed by infrared spectroscopy. *J. Am. Chem. Soc.* **2004**, *126*, 14239–14248.
8. Shima, S.; Lyon, E.J.; Sordel-Klippert, M.S.; Kauss, M.; Kahnt, J.; Thauer, R.K.; Steinbach, K.; Xie, X.L.; Verdier, L.; Griesinger, C. The cofactor of the iron-sulfur cluster free hydrogenase Hmd: Structure of the light-inactivation product. *Angew. Chem. Int. Ed.* **2004**, *43*, 2547–2551.
9. Shima, S.; Lyon, E.J.; Thauer, R.K.; Mienert, B.; Bill, E. Mössbauer studies of the iron-sulfur cluster-free hydrogenase: The electronic state of the mononuclear Fe active site. *J. Am. Chem. Soc.* **2005**, *127*, 10430–10435.
10. Hiromoto, T.; Ataka, K.; Pilak, O.; Vogt, S.; Stagni, M.S.; Meyer-Klaucke, W.; Warkentin, E.; Thauer, R.K.; Shima, S.; Ermler, U. The crystal structure of C176A mutated [Fe]-hydrogenase suggests an acyl- iron ligation in the active site iron complex. *FEBS Lett.* **2009**, *583*, 585–590.
11. Hiromoto, T.; Warkentin, E.; Moll, J.; Ermler, U.; Shima, S. The crystal structure of an [Fe]-hydrogenase-substrate complex reveals the framework for H_2 activation. *Angew. Chem. Int. Ed.* **2009**, *48*, 6457–6460.
12. Shima, S.; Schick, M.; Kahnt, J.; Ataka, K.; Steinbach, K.; Linne, U. Evidence for acyl–iron ligation in the active site of [Fe]-hydrogenase provided by mass spectrometry and infrared spectroscopy. *Dalton Trans.* **2012**, *41*, 767–771.
13. Korbas, M.; Vogt, S.; Meyer-Klaucke, W.; Bill, E.; Lyon, E.J.; Thauer, R.K.; Shima, S. The iron-sulfur cluster-free hydrogenase (Hmd) is a metalloenzyme with a novel iron binding motif. *J. Biol. Chem.* **2006**, *281*, 30804–30813.
14. Shima, S.; Schick, M.; Tamura, H. Preparation of [Fe]-hydrogenase from methanogenic archaea. *Methods Enzymol.* **2011**, *494*, 119–137.
15. Shima, S.; Vogt, S.; Göbels, A.; Bill, E. Iron-chromophore circular dichroism of [Fe]-hydrogenase: The conformational change required for H_2 activation. *Angew. Chem. Int. Ed.* **2010**, *49*, 9917–9921.

16. Lyon, E.J.; Shima, S.; Buurman, G.; Chowdhuri, S.; Batschauer, A.; Steinbach, K.; Thauer, R.K. UV-A/blue-light inactivation of the 'metal-free' hydrogenase (Hmd) from methanogenic archaea: The enzyme contains functional iron after all. *Eur. J. Biochem.* **2004**, *271*, 195–204.
17. Hidese, R.; Ataka, K.; Bill, E.; Shima, S. Cu^{I} and H_2O_2 Inactivate and Fe^{II} Inhibits [Fe]-hydrogenase at very low concentrations. *Chembiochem* **2015**, *16*, 1861–1865.
18. Huang, G.; Wagner, T.; Ermler, U.; Bill, E.; Ataka, K.; Shima, S. Dioxygen sensitivity of [Fe]-hydrogenase in the presence of reducing substrates. *Angew. Chem. Int. Ed.* **2018**, *57*, 4917–4920.
19. Buurman, G.; Shima, S.; Thauer, R.K. The metal-free hydrogenase from methanogenic archaea: Evidence for a bound cofactor. *FEBS Lett.* **2000**, *485*, 200–204.
20. Huang, G.F.; Wagner, T.; Wodrich, M.D.; Ataka, K.; Bill, E.; Ermler, U.; Hu, X.L.; Shima, S. The atomic-resolution crystal structure of activated [Fe]-hydrogenase. *Nat. Catal.* **2019**, *2*, 537–543.
21. Song, L.C.; Zhu, L.; Liu, B.B. A biomimetic model for the active site of [Fe]-H_2ase featuring a 2-methoxy-3,5-dimethyl-4-phosphato-6-acylmethylpyridine ligand. *Organometallics* **2019**, *38*, 4071–4075.
22. Seo, J.; Manes, T.A.; Rose, M.J. Structural and functional synthetic model of mono-iron hydrogenase featuring an anthracene scaffold. *Nat. Chem.* **2017**, *9*, 552–557.
23. Kerns, S.A.; Magtaan, A.C.; Vong, P.R.; Rose, M.J. Functional hydride transfer by a thiolate-containing model of mono-iron hydrogenase featuring an anthracene scaffold. *Angew. Chem. Int. Ed.* **2018**, *57*, 2855–2858.
24. Xu, T.; Yin, C.J.M.; Wodrich, M.D.; Mazza, S.; Schultz, K.M.; Scopelliti, R.; Hu, X. A functional model of [Fe]-hydrogenase. *J. Am. Chem. Soc.* **2016**, *138*, 3270–3273.
25. Pan, H.J.; Huang, G.F.; Wodrich, M.D.; Tirani, F.F.; Ataka, K.; Shima, S.; Hu, X.L. A catalytically active [Mn]-hydrogenase incorporating a non-native metal cofactor. *Nat. Chem.* **2019**, *11*, 669–675.
26. Hu, B.; Chen, D.; Hu, X.L. Synthesis and reactivity of mononuclear iron models of [Fe]-hydrogenase that contain an acylmethylpyridinol ligand. *Chem. Eur. J.* **2014**, *20*, 1677–1682.
27. Chen, D.; Scopelliti, R.; Hu, X. A five-coordinate iron center in the active site of [Fe]-hydrogenase: Hints from a model study. *Angew. Chem. Int. Ed.* **2011**, *50*, 5671–5673.
28. Shima, S.; Chen, D.; Xu, T.; Wodrich, M.D.; Fujishiro, T.; Schultz, K.M.; Kahnt, J.; Ataka, K.; Hu, X.L. Reconstitution of [Fe]-hydrogenase using model complexes. *Nat. Chem.* **2015**, *7*, 995–1002.
29. Schick, M.; Xie, X.L.; Ataka, K.; Kahnt, J.; Linne, U.; Shima, S. Biosynthesis of the iron-guanylylpyridinol cofactor of [Fe]-hydrogenase in methanogenic archaea as elucidated by stable-isotope labeling. *J. Am. Chem. Soc.* **2012**, *134*, 3271–3280.
30. Schwörer, B.; Thauer, R.K. Activities of formylmethanofuran dehydrogenase, methylenetetrahydromethanopterin dehydrogenase, methylenetetrahydromethanopterin reductase, and heterodisulfide reductase in methanogenic bacteria. *Arch. Microbiol.* **1991**, *155*, 459–465.
31. de Poorter, L.M.I.; Keltjens, J.T. Convenient fluorescence-based methods to measure membrane potential and intracellular pH in the Archaeon *Methanobacterium thermoautotrophicum*. *J. Microbiol. Methods* **2001**, *47*, 233–241.
32. Shima, S.; Thauer, R.K. Tetrahydromethanopterin-specific enzymes from *Methanopyrus kandleri*. *Methods Enzymol.* **2001**, *331*, 317–353.
33. Moore, J.T.; Uppal, A.; Maley, F.; Maley, G.F. Overcoming inclusion body formation in a high-level expression system. *Protein Expres. Purif.* **1993**, *4*, 160–163.
34. Virtanen, P.; Gommers, R.; Oliphant, T.E.; Haberland, M.; Reddy, T.; Cournapeau, D.; Burovski, E.; Peterson, P.; Weckesser, W.; Bright, J.; et al. SciPy 1.0: Fundamental algorithms for scientific computing in Python. *Nat. Methods* **2020**, *17*, 261–272.
35. Van der Walt, S.; Colbert, S.C.; Varoquaux, G. The NumPy Array: A structure for efficient numerical computation. *Comput. Sci. Eng.* **2011**, *13*, 22–30.
36. Hunter, J.D. Matplotlib: A 2D graphics environment. *Comput. Sci. Eng.* **2007**, *9*, 90–95.
37. McKinney, W. Data structures for statistical computing in Python. In Proceedings of the 9th Python in Science Conference, Austin, TX, USA, 28–30 June 2010; pp. 51–56.
38. Kabsch, W. Xds. *Acta Crystallogr. D* **2010**, *66*, 125–132.
39. Winn, M.D.; Ballard, C.C.; Cowtan, K.D.; Dodson, E.J.; Emsley, P.; Evans, P.R.; Keegan, R.M.; Krissinel, E.B.; Leslie, A.G.; McCoy, A.; et al. Overview of the *CCP*4 suite and current developments. *Acta Crystallogr. D* **2011**, *67*, 235–242.

40. McCoy, A.J.; Grosse-Kunstleve, R.W.; Adams, P.D.; Winn, M.D.; Storoni, L.C.; Read, R.J. Phaser crystallographic software. *J. Appl. Crystallogr.* **2007**, *40*, 658–674.
41. Emsley, P.; Lohkamp, B.; Scott, W.G.; Cowtan, K. Features and development of Coot. *Acta Crystallog. D* **2010**, *66*, 486–501.
42. Liebschner, D.; Afonine, P.V.; Baker, M.L.; Bunkóczi, G.; Chen, V.B.; Croll, T.I.; Hintze, B.; Hung, L.W.; Jain, S.; McCoy, A.J.; et al. Macromolecular structure determination using X-rays, neutrons and electrons: Recent developments in Phenix. *Acta Crystallogr. D* **2019**, *75*, 861–877.
43. Madeira, F.; Park, Y.M.; Lee, J.; Buso, N.; Gur, T.; Madhusoodanan, N.; Basutkar, P.; Tivey, A.R.N.; Potter, S.C.; Finn, R.D.; et al. The EMBL-EBI search and sequence analysis tools APIs in 2019. *Nucleic Acids Res.* **2019**, *47*, W636–W641.
44. Robert, X.; Gouet, P. Deciphering key features in protein structures with the new ENDscript server. *Nucleic Acids Res.* **2014**, *42*, W320–W324.